

## Article

# *Cissus antractica*-ZnO NPs Induce Apoptosis in A549 Cells through ROS-Generated p53/Bcl-2/Bax Signaling Pathways and Inhibition of Inflammatory Cytokines

Esrat Jahan Rupa <sup>1,†</sup>, Jinnatun Nahar <sup>2,†</sup>, Md. Al-Amin <sup>3,†</sup>, Jin-Kyu Park <sup>2</sup>, Mohanapriya Murugesan <sup>2</sup>, Muhammad Awais <sup>2</sup>, Seung-Jin Lee <sup>4</sup>, Il Mun Kim <sup>5</sup>, Li Ling <sup>2</sup>, Deok-Chun Yang <sup>1,2,6,7</sup>, Dong-Uk Yang <sup>6</sup>, Dae-Hyo Jung <sup>2,\*</sup> and Seok-Kyu Jung <sup>8,\*</sup>

- <sup>1</sup> Department of Oriental Medicinal Biotechnology, College of Life Sciences, Kyung Hee University, Yongin-si 17104, Republic of Korea; eshratrupa91@gmail.com (E.J.R.); dcyang@khu.ac.kr (D.-C.Y.)
  - <sup>2</sup> Graduate School of Biotechnology, College of Life Sciences, Kyung Hee University, Yongin-si 17104, Republic of Korea; pjinkyu53@gmail.com (J.-K.P.); priyabuddy44@gmail.com (M.M.); awaiskazmi@khu.ac.kr (M.A.); aqling@naver.com (L.L.)
  - <sup>3</sup> Department of Chemistry Education, Graduate Department of Chemical Materials, Pusan National University, Busan 46241, Republic of Korea
  - <sup>4</sup> Nature Bio Pharma Co., Ltd., Seoul 06241, Republic of Korea; lsjin0144@naver.com
  - <sup>5</sup> Pyeongtaek Medicinal Herb Farm, Pyeongtaek-si 17796, Republic of Korea; munkim607@naver.com
  - <sup>6</sup> Hanbangbio Inc., 13, Heungdeok 1-ro, Yongin-si 16954, Republic of Korea; rudckfeo23@naver.com
  - <sup>7</sup> State Local Joint Engineering Research Center of Ginseng Breeding and Application, Jilin Agriculture University, Changchun 130118, China
  - <sup>8</sup> Department of Horticulture, Kongju National University, Yesan 32439, Republic of Korea
- \* Correspondence: daxiao@daum.net (D.-H.J.); ungsk@kongju.ac.kr (S.-K.J.)  
† These authors contributed equally to this work.



**Citation:** Rupa, E.J.; Nahar, J.; Al-Amin, M.; Park, J.-K.; Murugesan, M.; Awais, M.; Lee, S.-J.; Kim, I.M.; Ling, L.; Yang, D.-C.; et al. *Cissus antractica*-ZnO NPs Induce Apoptosis in A549 Cells through ROS-Generated p53/Bcl-2/Bax Signaling Pathways and Inhibition of Inflammatory Cytokines. *Coatings* **2023**, *13*, 2077. <https://doi.org/10.3390/coatings13122077>

Academic Editors: Simona Liliana Iconaru and Laura DAlfonso

Received: 4 August 2023  
Revised: 7 December 2023  
Accepted: 9 December 2023  
Published: 13 December 2023



**Copyright:** © 2023 by the authors. Licensee MDPI, Basel, Switzerland. This article is an open access article distributed under the terms and conditions of the Creative Commons Attribution (CC BY) license (<https://creativecommons.org/licenses/by/4.0/>).

**Abstract:** Biogenic synthesis using medicinal plants has less harmful effects as compared to the chemical synthesis of nanoparticles. Here, for the first time, we successfully demonstrated the eco-friendly synthesis of zinc oxide nanoparticles (ZnO NPs) using an aqueous extract of *Cissus antractica*. The green synthesis method offers great potential for developing new medications that enhance drug bioavailability. The current work highlighted the cytotoxicity, cell death, and routes of apoptosis in lung cancer cells (A549) and inflammatory effects through synthesizing zinc oxide nanoparticles (ZnO NPs) from the *Cissus antractica* plant using an eco-friendly methodology. UV–visible (UV-Vis) spectroscopy, X-ray diffraction (XRD), transmission electron microscopy (TEM), Fourier-transform infrared spectroscopy (FT-IR), and energy-dispersive X-ray spectroscopy (EDS) were also used to characterize the synthesized ZnO nanoparticles. The average size of the NPs was 100 nm, and the NPs were crystalline in nature, as confirmed by FE-TEM and XRD analysis, respectively. In addition, the morphology of the nanoparticles analyzed by FE-TEM showed a spherical shape. The cell viability assay indicated that CA-ZnO NPs are non-toxic to normal cell lines at concentrations up to 20 µg/mL but showed significant toxicity in the A549 cell line. The nanoformulation also increased the ROS generation level in A549 lung cancer cells, and cellular apoptosis was confirmed via Hoechst and PI staining. The CA-ZnO NPs showed significant colony inhibition as well as cell migration ability that highlighted the CA-ZnO NPs as an anticancer agent. Additionally, this study demonstrated that NPs reduced the production of reactive oxygen species (ROS) and enhanced the expression of genes for BAX accumulation by releasing Cyto-c, but decreased Bcl-2 gene expression via the mitochondrial-mediated apoptosis pathway. In addition, the anti-inflammatory effect was also investigated; the CA-ZnO NPs showed significant NO inhibition ability with suppression of pro-inflammatory cytokines (TNF- $\alpha$ , iNOS, COX-2, IL-6, IL-8). In conclusion, *Cissus antractica* can be a source of significant Nano drugs with more advanced research in order to develop future anti-inflammatory and anticancer medications.

**Keywords:** *Cissus antractica*; ZnO NPs; anti-lung cancer; anti-inflammation; apoptosis

## 1. Introduction

As part of the immune system, inflammation can be caused by a variety of factors, such as pathogens, damaged cells, and toxins [1]. To stop the spread of diseases, the body naturally uses inflammation as a defense mechanism [2]. A local immune, vascular, and inflammatory cell response to infection or injury leads to inflammation at the tissue level. These cells cause redness, swelling, heat, pain, and loss of tissue function [3]. There are different mediators and cytokines involved in inflammation. When inflammatory mediators and cytokines are released, the immune system's other cells are activated and go toward the area of inflammation, starting an inflammatory response [4]. The activation and production of free radicals like reactive oxygen and nitric oxide from various immune system cells including neutrophils and macrophages may result in tissue damage and lipid peroxidation [5]. The release of mediators and lytic enzymes from macrophages results in tissue damage and lipid peroxidation due to the produced reactive oxygen species and nitric oxide [6]. Uncontrolled inflammation leads to DNA damage and mutations, which in turn promote the growth of malignant cells. Numerous inflammatory mediators, including interferons, interleukins, and tissue necrosis factors, promote tumors [7]. Globally, cancer accounts for the first leading cause of death, and it is caused by a variety of factors, including genetics and the environment [8]. Almost 20% of all cancer patients die of lung cancer all over the world [9]. Small-cell lung cancer (SCLC) and non-small-cell lung cancer (NSCLC) are the two primary subtypes of lung cancer. SCLC accounts for 15% of total cases, while NSCLC accounts for 85% [10]. Lung cancer was the second most prevalent cancer diagnosed by 2020 (11.4% of all cases), and it was also the major cause of cancer death (18%, 1.8 million fatalities) [11]. Radiation therapy, chemotherapy, hormone therapy, and surgery are used together to treat and manage the majority of cancers. Nevertheless, there are several disadvantages to using these strategies despite their historic success. Additionally, radiation or chemotherapy has severe negative effects on cancerous patients [12]. Therefore, it is urgently necessary to discover alternative in current cancer research.

Recently, bioengineered nanomaterials, more specifically, nanotechnology, have gained popularity as a superior form of biodegradable material for a variety of medical uses, including the diagnosis and treatment of various illnesses [13]. Recently, researchers have been studying green chemistry methods for synthesizing metal nanoparticles to design and develop the most efficient and eco-friendly methods [14]. Nanoparticles may be produced using a variety of processes, including chemical, physical, and biological mechanisms. The use of bio-resources (plants, fungi, algae, and microorganisms) that can act as reducing, stabilizing, and capping agents makes the green synthesis approach for the synthesis of metal nanoparticles one of many methods available in the literature that has several advantages over conventional methods, such as biocompatibility, low toxicity, ease of manufacturing, cost-effectiveness, and the ability to control the synthesis process [15]. As a result of their exceptional physical and chemical properties, zinc oxide nanoparticles (ZnO NPs) are also widely employed in a variety of fields [16]. ZnO NPs offer a wide range of medical applications compared to other metal oxide nanoparticles, including drug delivery, anticancer, antibacterial, anti-inflammation, diabetic treatment, wound healing, and bioimaging applications [17,18]. ZnO NPs that are 100 nm in size are regarded as biocompatible and substantial. ZnO NPs are prospective medications since they are generally recognized as safe (GRAS) and have received approval from the US Food and Drug Administration (FDA) for other delivery options [19].

People have relied on natural cures as their primary source of medicine throughout human history [20]. Since prehistoric times, plant-based medications have served as the foundation of traditional medical practices used in many nations, including Egypt, India, and China [21]. Due to their unique effectiveness, safety, and economic impact on cancer, natural products today play an important role in cancer prevention and therapy [22]. With approximately 300 species dispersed over all of the major tropical zones, *Cissus* is the biggest genus in the Vitaceae family of grapes [23]. One of the most well-known

species of the genus *Cissus* in the family Vitaceae is *Cissus antarctica*, sometimes known as “kangaroo vine” [24]. *Cissus antarctica* is a yellowish leaf, with an ovate to ovate-oblong lamina, mostly 4–12 cm long and 20–50 mm wide, used traditionally as a vine in subtropical climates and as an ornamental plant in gardens. *Cissus* species contain saponins, triterpenoids, terpenoids, alcohols, phenols, alkanes, carboxylic acids, alkenes, aliphatic amines, and aromatics [25,26]. Extracts from *Cissus* species such as *Cissus quadrangular*, *Cissus rhombifolia*, *Cissus incisa*, and *Cissus cornifolia* have been reported to have beneficial effects on human health as antioxidant, antimicrobial, anticancer, neuroprotective, antibacterial, and anti-inflammatory agents [27–29] as well as nanoformulations [30,31], but there is no scientific evidence that *Cissus antractica* is pharmacologically efficacious against lung cancer and inflammation.

Physicochemical techniques were used to elucidate the morphology and chemical composition of nanoparticles produced using green synthesis. In addition, reactive oxygen species are external mediators that support several signaling pathways, including those that contribute to the development and spread of cancer [32]. Previous studies showed that the p53 signaling pathway might be used by ROS to control cancer growth and apoptosis [33]. As a result, numerous pro-inflammatory cytokines, including interleukin-4 (IL-4), interleukin-6 (IL-6), interleukin-8 (IL-8), and interleukin-10 (IL-10), signal to the NF- $\kappa$ B signaling pathway. Therefore, the apoptosis and reduced pro-inflammatory cytokines of the aforementioned targets play important roles in inflammation and lung cancer therapy.

More study is now required on the relevance of biologically active compounds obtained from natural resources with nanoparticles, such as chemicals with qualities that may reduce cancer risk and inflammation. However, anti-inflammatory and anti-lung-cancer activity in A549 cell lines and RAW 264.7 have not been reported yet. Therefore, this study was planned to formulate zinc oxide nanoparticles from an extract of *Cissus antractica*, and there in vitro anticancer and anti-inflammatory actions were examined against lung cancer macrophage cells.

## 2. Materials and Methods

### 2.1. Chemicals

The dried leaves of *Cissus antractica* were collected from Nature Garden, Republic of Korea. Samchun Pure Chemical Co. Ltd. (Pyeongtaek-si, Republic of Korea) provided the absolute alcohol, sodium hydroxide (>98.0%), and zinc nitrate hex hydrate ( $\text{Zn}(\text{NO}_3)_2 \cdot 6\text{H}_2\text{O}$ ; >98.0%) for the experiment. We bought a human lung cancer cell line (A549) and the murine macrophage RAW 264.7 cell line from the Korean Cell Line Bank (KCLB, Seoul, Republic of Korea), and these cell lines were used in this experiment. In addition, 10% fetal bovine serum (FBS), 1% penicillin/streptomycin, Roswell Park Memorial Institute (RPMI) 1640, and Dulbecco’s Modified Eagle Medium (DMEM) culture medium were purchased from Welgene Inc. in Gyeongsan-si, Republic of Korea. We purchased the MTT reagent from Life Technologies in Eugene, OR, USA. A reader for ELISA was used. All reagents were of analytical grade and used as they were received.

### 2.2. Preparation of *Cissus antractica* Water Extract

The samples were collected, washed, and dried with a dehydrator for 20 h at 35 °C. The whole plant was ground into a fine powder using a grinder. Further, 1 g of dried powder was diluted in distilled water and sonicated for 140 min. Then, it was transferred to a hot extraction water bath for 30 min. A rotary evaporator was used for drying and reaching the final extract concentration of 20 mg/mL. Further, the extract was freeze-dried and stored at 4 °C (Figure 1).

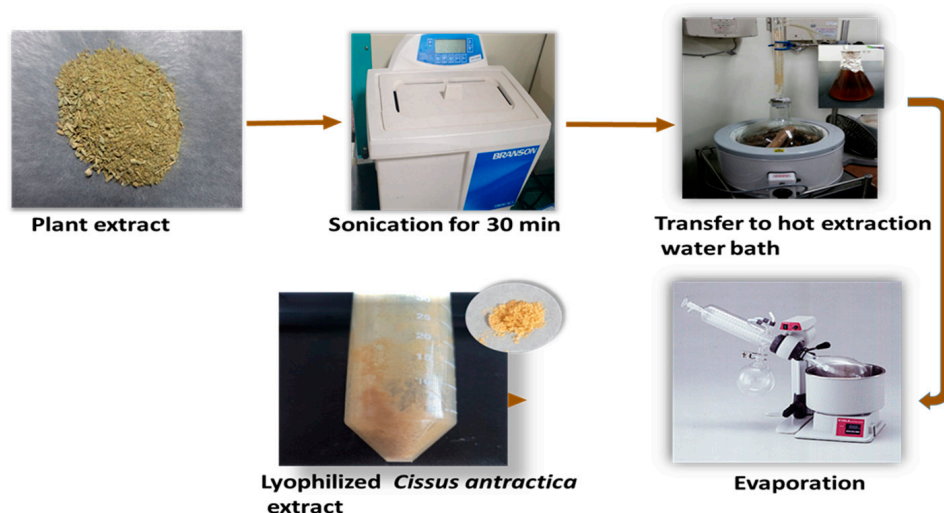


**Figure 1.** *Cissus antractica* plant extract preparation.

### 2.3. ZnO NPs Using Co-Precipitation Method

The ZnO NPs were synthesized using the co-precipitation method with sodium hydroxide and zinc nitrate salt as a reducing agent. The sample (10% extract) was placed on a hot plate with a magnetic stirrer and heated to 50 °C with continuous agitation. Drop by drop, zinc nitrate (0.1 M) and sodium hydroxide (0.2 M) were added and left undisturbed for two hours. After synthesis, the nanoparticles were collected by centrifugation at 5000 rpm for 10 min, twice. The synthesized nanoparticles were kept in a 60 °C oven for four hours and kept at 4 °C for the next steps of the experiment (Figure 2).

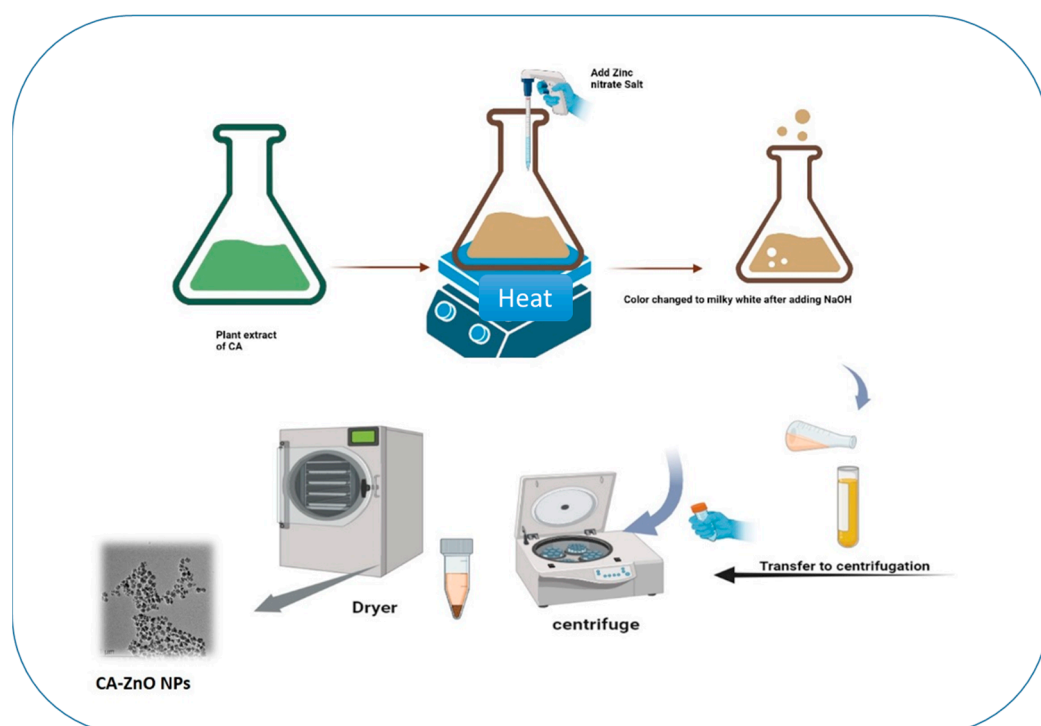


**Figure 2.** Synthesis of CA-ZnO NPs.

### 2.4. Characterization of ZnO Nanoparticles

To determine the structural and optical characteristics of the synthesized CA-ZnO nanoparticles, various analytical instruments were used to identify the shape, exact size, purity, and nature of the nanoparticles.

#### 2.4.1. UV-Vis Spectrophotometry

UV-visible spectroscopy in the 200 to 800 nm range (Ultra-spec TM-2100 Pro) revealed the effective formation of ZnO NPs.

#### 2.4.2. FT-IR Spectroscopy

The spectra of powdered zinc oxide nanoparticles were examined using an FT-IR apparatus (PerkinElmer Inc., Waltham, MA, USA). Plots of transmittance (%) vs. wavenumber ( $\text{cm}^{-1}$ ) show spectral characteristics.

#### 2.4.3. XRD Analysis

X-ray diffraction (D8 Advance, Bruker, Germany) was used to determine the crystallinity and specific size of CA-ZnO nanoparticles. The detector voltage was 40 kV, the current was 40 mA, and the Cu-K radiation was 1.54. Rapid scanning ( $6^\circ/\text{min}$ ) was used to record properties in the  $2^\circ$  range of  $20\text{--}80^\circ$ .

#### 2.4.4. FE-TEM Analysis

The morphological investigation and particle size distribution analysis were carried out using TEM (200 kV) (JEM-2100F (JEOL, Tokyo, Japan)). The particle size was calculated using ImageJ software (<https://imagej.net/ij/>) after the various TEM images were digitized. A copper grid coated with a thin layer of carbon was used for TEM analysis.

### 2.5. Cell Culture

Human lung cancer (A549) was created using a growth medium that contained 89% RPMI 1640, 10% FBS, and 1% P/S. The standard culture medium for murine macrophage (RAW 264.7) cells was DMEM with 10% FBS and 1% penicillin–streptomycin. A549 and RAW 264.7 cell lines were permitted to attach and grow for one day in a humid incubator at 37 degrees with 5%  $\text{CO}_2$  before being exposed to different substances.

### 2.6. Cytotoxicity Assay

The cytotoxicity of cisplatin, zinc salt, CA-Ex, and CA-ZnO NPs was examined in A549 and RAW 264.7 cell lines by employing a cytotoxicity assay. The toxicity of cisplatin (20  $\mu\text{M}$ ) was tested in only A549 cells, and the results were compared to those for zinc salt, CA-Ex, and CA-ZnO NPs after one day. Both cancer cells and healthy cells were first plated in a 96-well plate at a decided-on density of  $1 \times 10^4$  cells/well. Cells were then exposed to a range of concentrations (0, 5, 10, 15, 20, 25, and 30  $\mu\text{g}/\text{mL}$ ) and allowed to incubate for 24 h. Cells were subjected to a treatment of 20  $\mu\text{L}$  of 3-(4, 5-dimethyl-2-thiazolyl)-2, 5-diphenyl tetrazolium bromide solution (MTT; 5 mg/mL, in PBS) after 24 h for 3–4 h at  $37^\circ\text{C}$ . Additionally, the presence of the MTT reagent causes live cells to produce purple formazan. To dissolve the insoluble formazan agents, 100  $\mu\text{L}$  of DMSO was added to each well. ELISA at 570 nm was used to collect the data.

### 2.7. Reactive Oxygen Species (ROS) Assay

To quantify ROS, 2',7'-dichlorodihydrofluorescein diacetate (DCFH-DA) was used on human lung carcinoma (A549). We placed the cells in 96-well cell culture plates at a density of  $1 \times 10^4$  cells per well and left them to reach 100% growth confluency the next day. The cells were stained with 100  $\mu\text{L}$  of DCFH-DA (10  $\mu\text{M}$ ) solution in each well after 24 h of treatment, and they were then allowed to sit in the dark for 30 min. The cells were then washed twice with PBS (100  $\mu\text{L}/\text{well}$ ), and the old medium was discarded. A multi-mode plate reader with an excitation wavelength of 485 nm and an emission wavelength of 528 nm was used to measure the fluorescence intensity of ROS production.

### 2.8. Colony Formation Assay

The A549 lung cancer cells were seeded at a concentration of  $1 \times 10^3$  on 6-well plates, and after 48 h, the cells were treated with several concentrations (15, 20  $\mu\text{g}/\text{mL}$ ) of CA-Ex and CA-ZnO NPs along with cisplatin (20  $\mu\text{M}$ ). After one day, the old cell medium was taken away and replaced with a fresh medium for the three-day incubation period (37  $^\circ\text{C}$ , 5%  $\text{CO}_2$ ). The colony was fixed with 4% formaldehyde (15 min) and stained with crystal violet dye (15 min). Additionally, colony counts were counted and evaluated using Image J software.

### 2.9. Wound-Healing Assay

The ability of the A549 cancer cells to migrate was examined in an experiment on wound healing. A549 lung cancer cells were seeded in 6-well plates at a density of  $2 \times 10^4$  cells/well, and the plates were then left to incubate at 37  $^\circ\text{C}$  for twenty-four hours. A 200  $\mu\text{L}$  sterile pipette tip was used to scrape the monolayer vertically, and any isolated cells were removed with PBS. After 72 h of treatment, cells were then exposed to varied doses of CA-Ex, CA-ZnO NPs (15 and 20  $\mu\text{g}/\text{mL}$ ), and cisplatin (20  $\mu\text{M}$ ). A 5.0-megapixel MC 170 HD camera (Wetzlar, Germany) embedded within the device was used to take pictures.

### 2.10. Hoechst Staining

A Hoechst-33342 staining kit was utilized to evaluate the induction of cisplatin (20  $\mu\text{M}$ ), CA-Ex, and CA-ZnO NPs during apoptosis in the A549 cancer cell line. In this case, cells were plated into a 6-well plate at a density of  $1 \times 10^4$  cells/well, with the addition of 2 mL of culture medium, and incubated for 24 h. Agents containing 4% paraformaldehyde were administered for 10 min (twice) after the treated cells had been cleaned with a 1 X PBS solution. After the Hoechst dye was added, the mixture was maintained at 37  $^\circ\text{C}$  for 10 min. After three PBS solution washes, the labeled cells were examined under a fluorescence microscope (Leica DMLB, Wetzlar, Germany) to capture images of the dying cells.

### 2.11. PI Staining

Cisplatin (20  $\mu\text{M}$ ), CA-Ex, and CA-ZnO NPs (15 or 20  $\mu\text{g}/\text{mL}$ ) were applied to seeded cells. Cells were treated for 24 h before being rinsed with 1 mL of PBS and stained for 10 min at room temperature with 500  $\mu\text{L}$  of propidium iodide reagent (5  $\mu\text{g}/\text{mL}$ ) solution. A fluorescent microscope (Leica DMLB, Wetzlar, Germany) was used to check the cells.

### 2.12. Quantitative Reverse Transcription PCR (qRT-PCR)

Following the manufacturer's instructions, 1  $\mu\text{g}$  of total RNA was added to 20  $\mu\text{L}$  of reaction buffer. To perform qRT-PCR, SYBR TOP real qPCR2X Premix (Enzynomics, Daejeon, Republic of Korea) was utilized. In a nutshell, the reactions were carried out in triplicate and contained 10  $\mu\text{L}$  of final solution, 2 $\times$  Master Mix, 1  $\mu\text{L}$  of template cDNA, and 1  $\mu\text{L}$  of forward and reverse primers. The aCFX Connect Real-Time PCR (Bio-Rad, Hercules, CA, USA) was employed for all real-time analyses. To increase the reactions, the following conditions were used: 95  $^\circ\text{C}$  for 10 min, followed by 40 cycles of 95  $^\circ\text{C}$  for 20 s and 55–60  $^\circ\text{C}$  for 30 s, followed by 15 s at 72  $^\circ\text{C}$ . Using the comparative  $2^{-\Delta\Delta\text{Ct}}$  technique, the relative amounts of mRNAs were determined and normalized using the GAPDH gene. The primer sequences (GenoTech, Daejeon, Republic of Korea) are shown in Table 1.

**Table 1.** Primer sequences for qRT-PCR mRNA gene expression analysis.

Gene	Primer Sequences (5'-3')
<i>p53</i>	F: TCT TGGGCC TGT GTT ATC TCC R: CGC CCA TGC AGG AAC TGT TA
<i>Bcl2</i>	F: GAA GGG CAG CCG TTA GGAAA R: GCG CCC AAT ACG ACC AAA TC

Table 1. Cont.

Gene	Primer Sequences (5'-3')
<i>BAX</i>	F: GGT TGC CCT CTT CTA CTT T R: AGC CAC CCT GGT CTT G
<i>CASPASE 3</i>	F: GAA GGA ACA CGC CAG GAA AC R: GCA AAG TGA AAT GTA GCA CCA A
<i>CASPASE 9</i>	F: GCC CGA GTT TGA GAG GAA AA R: CAC AGC CAG ACC AGG AC
<i>Cyto-c</i>	F: CAGAAGGAAGTTAGGCC R: CGTCGCAGTGGATGATGTG
<i>COX-2</i>	F: CCT GAG CAT CTA CGG TTT GC R: ACT GCT CAT CAC CCC ATT CA
<i>TNF-<math>\alpha</math></i>	F: GCCAGAATGCTGCAGGACTT R: GGCCTAAGTCCACTTGTGTCA
<i>iNOS</i>	F: CCT GAG CAT CTA CGG TTT GC R: ACT GCT CAT CAC CCC ATT CA
<i>IL-6</i>	F: AGGGTTGCCAGATGCAATAC R: AAACCAAGGCACAGTGGAAAC
<i>IL-8</i>	F: CCGGAGAGGAGACTTCACAG R: GGAAATTGGGGTAGGAAGGA
<i>GAPDH</i>	F: CAA GGT CAT CCA TGA CAA CTT TG R: GTC CAC CAC CCT GTT GCT GTA G

### 3. Results and Discussion

#### 3.1. Synthesis of CA-ZnO NPs

The ZnO NPs were synthesized using the whole plant via the co-precipitation method due to significant advantages such as its short procedure time, eco-friendliness, low cost, and avoidance of toxic chemicals resulting in fewer side effects.

#### 3.2. Characterization of CA-ZnO NPs

The shape, specific size, and stability of the produced ZnO nanoparticles, as well as their structural and optical properties, were assessed using a variety of characterization instruments.

#### 3.3. UV-Vis Spectral Analysis

The UV-visible spectrum absorption spectra were used to determine the optical properties of CA-ZnO NPs. The synthesized CA-ZnO NPs and the *Cissus antractica* whole plant extract are shown in Figure 3. The sharp peak in the absorption spectrum at 360 nm (Figure 3) confirmed the formation of ZnO NPs from the plant extract.

The UV-visible wavelength range was between 200 and 800 nm. The wide absorption band that extends to longer wavelengths may be caused by the migration of the electronic cloud on the general skeleton of the ZnO NPs. The plant extract was also subjected to UV-Vis analysis, which revealed several peaks at various wavelengths that extend from 300 to 600 nm (Figure 3) owing to the presence of phytochemicals (proteins and antioxidant molecules). Because of the presence of these molecules in the plant extract, Zn metal salt was reduced to create ZnO NPs.

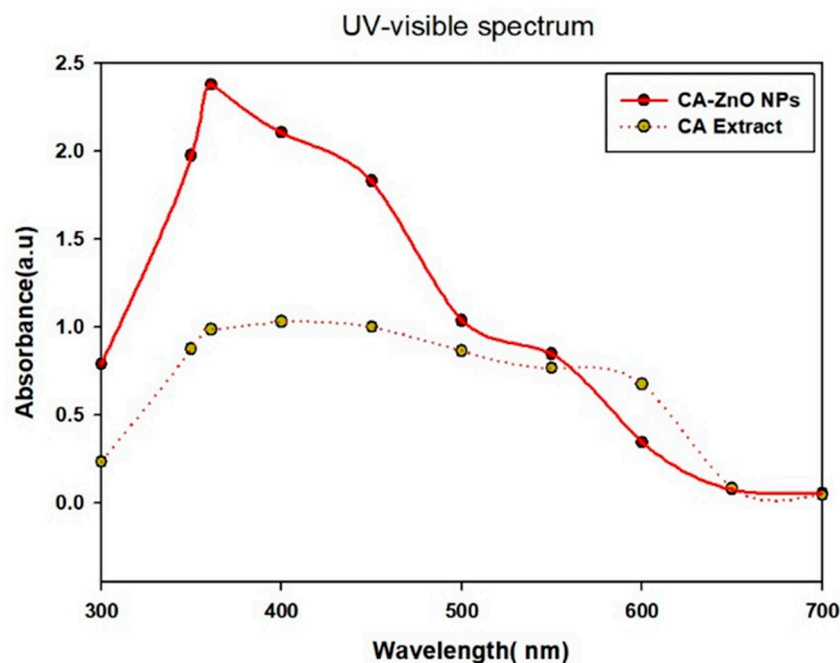


**Figure 3.** UV-Vis analysis of CA-ZnO NPs.

### 3.4. FE-TEM and EDX Analysis

The morphological characterization of CA-ZnO NPs was performed using transmission electron microscopy (TEM). The ideal technique for directly measuring morphology, size distribution, grain size, and nanoparticle size is TEM [15]. The ZnO NPs revealed a cotton-form structure on the 50 nm and 100 nm scale bars in the FE-TEM pictures, which depict the morphology. The size of the nanoparticles was shown in DLS analysis with a PDI value and was in the range of 110–152 nm. In the image regarding the size of the individual particles, it is shown that the average size is less than 100 nm. The DLS size is larger due to the hydrodynamic nature of the nanoparticles resulting in a swelling effect in water. Figure 4a–c show the details of the morphology and structure of CA-ZnO NPs that were synthesized from *Cissus antractica* obtained by FE-TEM and SAED monographs. Metal nanoparticles are mostly crystalline in nature; a ZnO NP is characterized as a semiconductor due to a wide band gap. Figure 4e–g show the elemental mapping, where the green dot represents the presence of Zn and the red dot represents oxygen. Moreover, in Figure 4h, the EDX spectrum represents the elemental identity, showing Zn and O without any other metal contamination. The EDX and elemental mapping showed that the synthesized ZnO NPs are pure in nature and that there is no other metal contamination. The weight percentages for Zn and O are 35.36 and 64.64, and the atomic percentages are 69.08 and 30.92, respectively (Table 2). Additionally, the SAED ring structure corroborated the crystalline structure of the ZnO NPs by matching the FWHM of the XRD structure, and the morphology provides strong evidence for this (Figure 4i). Sharp peaks shown in the spectrum were associated with zinc and oxygen, including two significant peaks [34]. In keeping with previous references, the existence of Zn and O was verified by a substantial peak signal of both metals in the EDX spectrum, confirming the presence of metal oxide nanoparticles and proving the lack of aggregation [35].

**Table 2.** The weight percentage of Zn and O with the atomic percentage.

Element	Weight %	Atomic %
O K	35.36	69.08
Zn K	64.64	30.92
Totals	100.00	

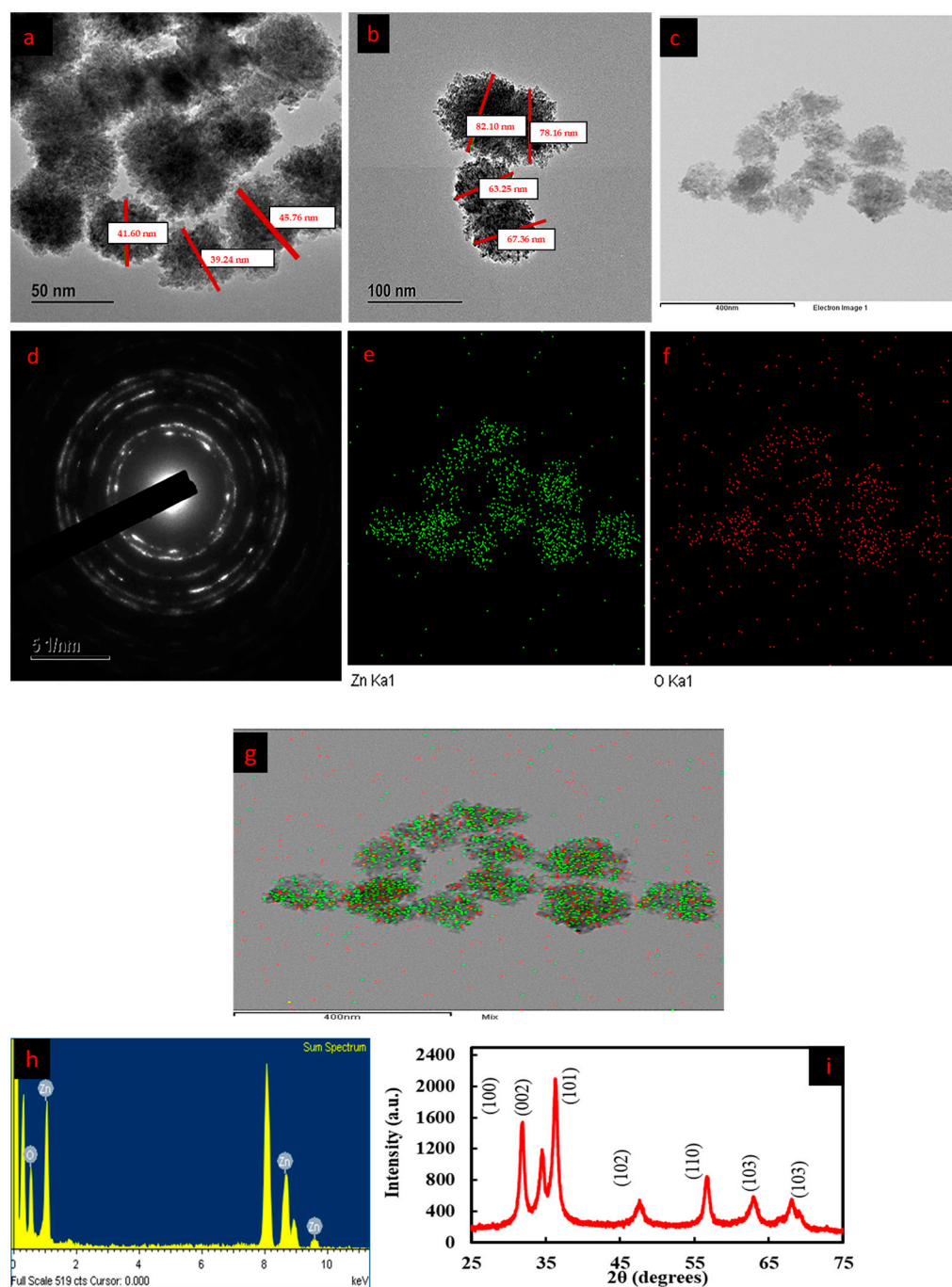


**Figure 4.** (a,b,d) FE-TEM images with different scale bars, (c) SAED of CA-ZnO NPs, (e–g) elemental analysis, (h) EDX analysis, and (i) XRD analysis of CA-ZnO NPs.

### 3.5. Fourier-Transform Infrared (FT-IR) Spectroscopy Analysis

Fourier-transform infrared spectroscopy was employed to detect the phytochemicals responsible for reducing  $Zn^{2+}$  and stabilizing the ZnO NPs. By examining the IR spectra, it is possible to determine how the sample compounds interact with the absorption bands [36]. As shown in Figure 5, in the region of  $3500\text{--}450\text{ cm}^{-1}$ , the FT-IR spectrum was used to classify the functional groups of the CA extract and CA-ZnO NPs (Figure 5). The hydroxyl group ( $-OH$ ) might be assigned to the high absorption peak seen at about  $3420\text{ cm}^{-1}$ . Alkane ( $-CH$ ), stretching, and alcohol ( $-C=O$ ) were attributed to weaker bands that were seen at roughly  $2850$  and  $2350\text{ cm}^{-1}$ . The existence of signals at  $1500\text{ cm}^{-1}$  corroborated the stretching vibration ( $-C=C$ ). Due to the production of zinc nanoparticles, the  $-OH$  group

was significantly reduced in the CA-ZnO NPs as compared to CA extract and CA-ZnO NP absorptions. The FT-IR measurements show that the manufactured ZnO NPs are remarkably pure [37].

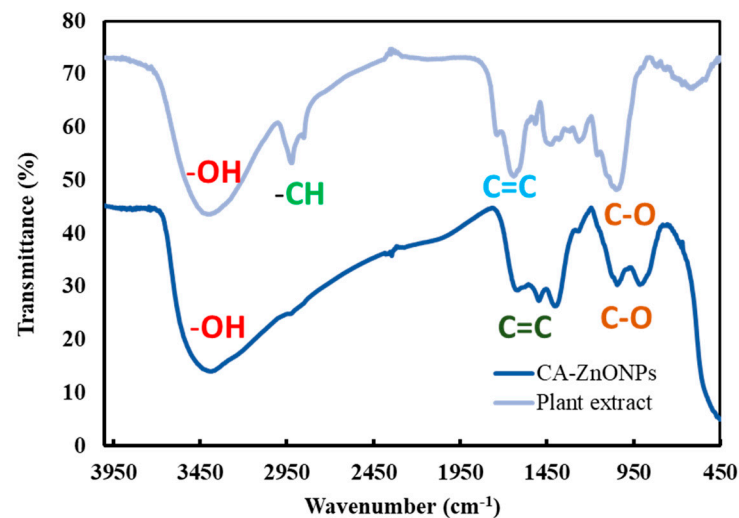


**Figure 5.** Functional group analysis of CA ZnO NPs by FT-IR spectroscopy.

### 3.6. Particle Size Distribution Analysis

The particle size distribution of CA-ZnO NPs was examined utilizing the dynamic light scattering (DLS) technique. DLS research revealed that CA-ZnO NPs had a hydrodynamic Z-average of 251 nm and a polydispersity index (PDI) of 0.173 (Figure 6 A). The hydrodynamic size that was achieved corresponded to the particle size range of 500–1000 nm. The PDI value indicated that the particles are monodisperse in nature, and the Z-average value indicated that the true hydrodynamic diameter was 151.51 nm (50 nm scale bar), as shown in FE-TEM analysis (Figure 6B).

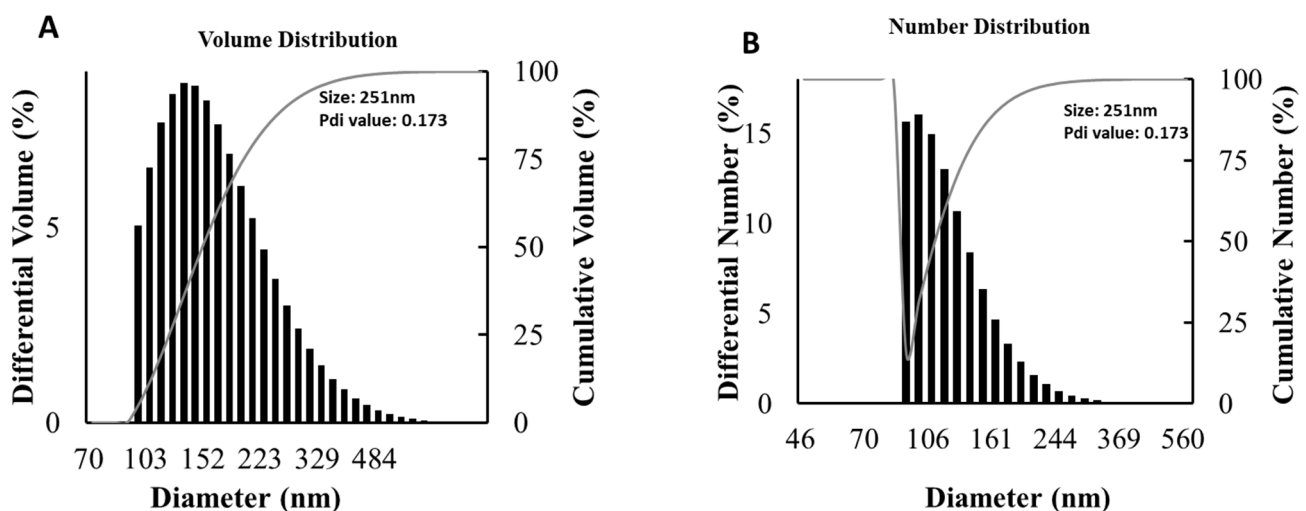


**Figure 6.** Size distribution of CA-ZnO NPs as determined by DLS analysis: (A) volume distribution; (B) number distribution.

### 3.7. Evaluation of Cell Cytotoxicity

ZnO NPs are popular carriers in the treatment of cancer. With their ability to target cancer cells specifically and their usefulness as anticancer drug carriers, ZnO nanoparticles can be an effective alternative to current cancer treatments. The anticancer activity of various doses of CA-ZnO NPs (0, 5, 10, 15, 20, 25, and 30  $\mu\text{g}/\text{mL}$ ) was evaluated using

the MTT assay. The positive control was a commercial cisplatin (20  $\mu\text{M}$ ) solution, while the control was untreated cells. CA-ZnO NPs dramatically reduced the proliferation of cancer cells by around 60% at a concentration of 20  $\mu\text{g}/\text{mL}$  when compared with ZnO salt and the plant extract (Figure 7B). In the meantime, RAW cells were also treated with different concentrations (0–30  $\mu\text{g}/\text{mL}$ ) of CA-ZnO NPs and showed around 12% less cell toxicity at 20  $\mu\text{g}/\text{mL}$  compared with the control (Figure 7A). The key processes behind the cytotoxicity of ZnO NPs are the intracellular release of dissolved zinc ions and the consequent production of reactive oxygen species (ROS) [38]. Extracellular ZnO is biocompatible; however, intracellular ZnO at higher doses exhibits greater cytotoxicity due to zinc-mediated protein activity disequilibrium and oxidative stress [39]. Furthermore, zinc oxide nanoparticles have been shown to destroy cancer cells by creating ROS on their surfaces. Because of the direct contact of nanoparticles with a cancer cell membrane, which results in oxidative stress and eventually leads to cancer cell death, the released  $\text{Zn}^{2+}$  ions are spread in the culture medium [40]. ZnO NPs have the capacity to quickly penetrate cells and disrupt mitochondria and specific DNA sequences, dramatically reducing tumor growth [41]. Hence, plant-extract reduced metal-capped nanoparticles become an effective way to treat cancer.

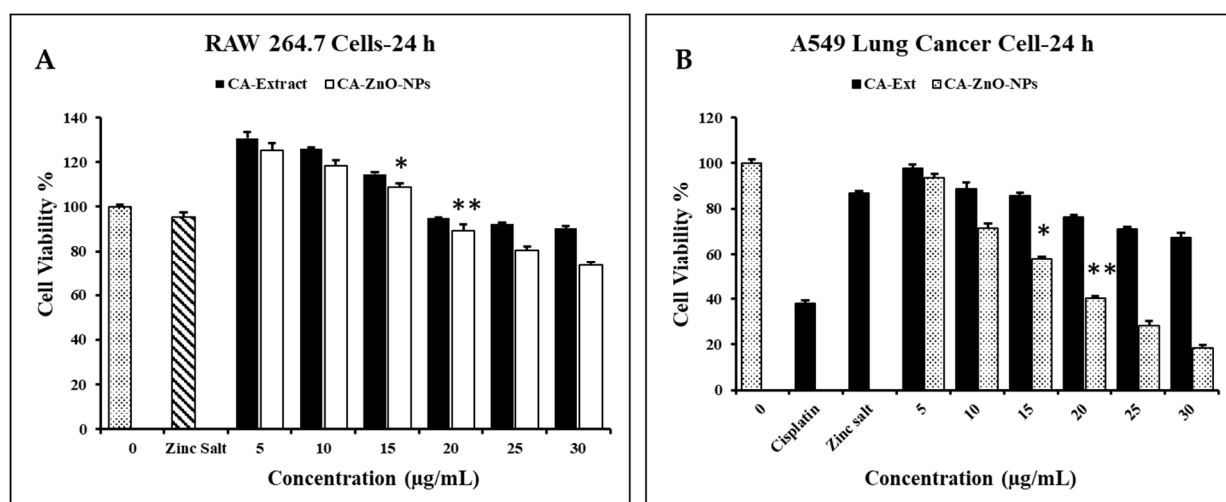


**Figure 7.** Percent cell viability was determined by MTT assay. Graphs representing percent cell viability of (A) Raw 264.7 and (B) A549 cells upon treatment with cisplatin, zinc salt, CA extract, and CA-ZnO NPs. The graph shows mean  $\pm$  SD values of four replicates. \*  $p < 0.01$ ; \*\*  $p < 0.001$  indicates significant differences from control groups.

### 3.8. In Vitro ROS Induced by CA-ZnO NPs in Cancer Cells

Due to the generation of higher levels of reactive oxygen species (ROS), ZnO nanoparticles become a significant carrier for anticancer treatment. In this study, the DCFH-DA reagent was used in A549 cells together with cisplatin, zinc salt, CA extract, and CA-ZnO NPs at various doses to measure the intracellular ROS level.

The ZnO nanoparticles can release zinc ions and oxygen vacancies and work as a potential donor/acceptor. A hole ( $h^+$ ) decomposes water molecules into hydrogen and hydroxyl ions. Similar to this, electrons interact with oxygen molecules that are adsorbed and dissolved to produce superoxide radical anions ( $\text{O}_2^-$ ). These superoxide radical anions then combine with hydrogen ions to form  $\text{HO}_2^-$  radicals, which then combine with oxygen atoms to form  $\text{H}_2\text{O}_2$  [42]. In order to drive redox reactions and the production of ROS in cellular environments, a sufficiently significant band gap must exist between the ZnO's conduction and valence. As a result, the ZnO nanoparticles create holes and electrons to cause redox reactions and produce reactive oxygen species, which raises oxidative stress in the cell [43]. Additionally, the potential mechanism underlying the specific cytotoxicity

of pH-responsive zinc oxide nanoparticles against cancer cells includes oxidative stress (through ROS formation) and subsequent cell damage.

Oxidative stress is caused by the pH-dependent quick breakdown of ZnO NPs into the release of  $Zn^{2+}$  ions under an acidic intracellular environment, and when compared to healthy cells, cancer cells produce more ROS; this increased ROS level eventually leads to mitochondrial malfunction and triggers the intrinsic mitochondrial apoptotic pathway [44]. However, as shown in Figure 8, CA-ZnO NPs produced more ROS at a concentration of 20  $\mu\text{g}/\text{mL}$  compared to the CA extract and zinc salt. ZnO nanoparticles' insolubility criterion resulting in the release of  $Zn^{2+}$  (greater concentration) was generally responsible for the cell cytotoxicity that was observed. When the ROS ratio exceeds the level of the cell's antioxidant defenses, the characteristics of ZnO NPs can produce ROS leading to cell death [45].

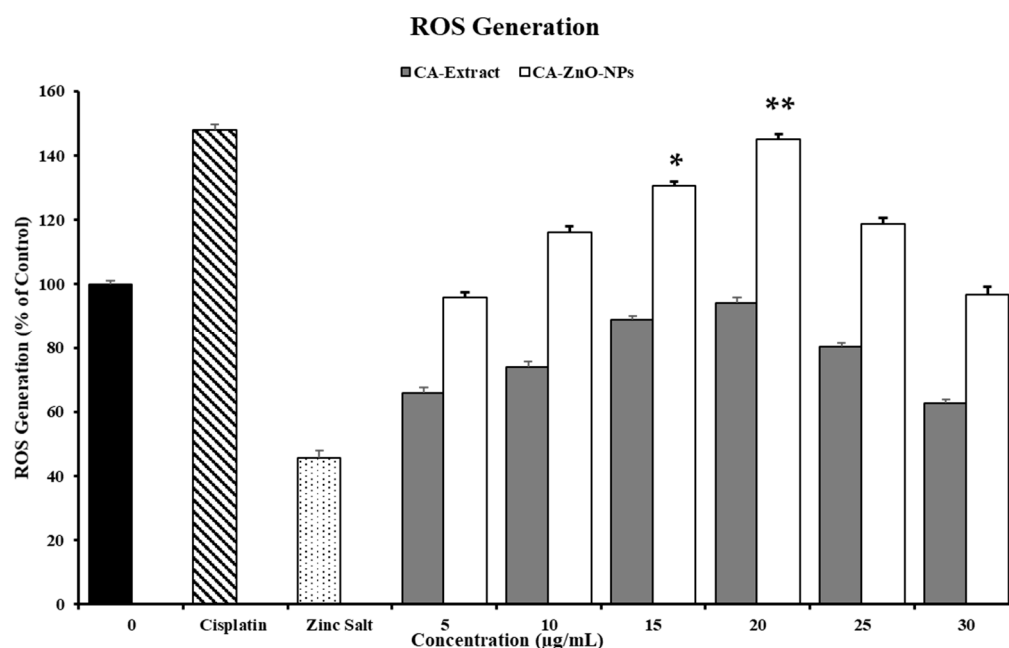


**Figure 8.** ROS determination by DCFH-DA staining in A549 cells treated with zinc salt, CA extract, and CA-ZnO NPs for 24 h. Cisplatin (20  $\mu\text{M}$ ) was used as a positive control. The graph shows the mean  $\pm$  SD values of three replicates. \*  $p < 0.05$ ; \*\*  $p < 0.001$  indicates significant differences from control groups.

### 3.9. Inhibition of Colony Formation of Cancer Cells

An in vitro cell survival test called the clonogenic assay (also known as the colony formation assay, or CFA) assesses a cell's capacity to form colonies [46]. Using this assay, drugs can be tested in vitro for their effects on cell growth and proliferation. The A549 cells' morphology and colony formation were evaluated using microscopic examination, as illustrated in Figure 9. The non-treated cells had more colonies than cells treated with CA-Ex and CA-ZnO NPs at 15 and 20  $\mu\text{g}/\text{mL}$ . In contrast, the number of colonies in the CA-ZnO NP group was smaller than that in the CA-Ex group. Additionally, using 20  $\mu\text{g}/\text{mL}$  of CA-ZnO NPs significantly reduced colony formation compared to untreated cells in 15 and 20  $\mu\text{g}/\text{mL}$ . These findings suggest that CA-ZnO NPs have the ability to promote the decolonization of cancer cells, proving their anticancer properties. The sample was compared with the commercial drug cisplatin, and the results suggested almost similar findings.

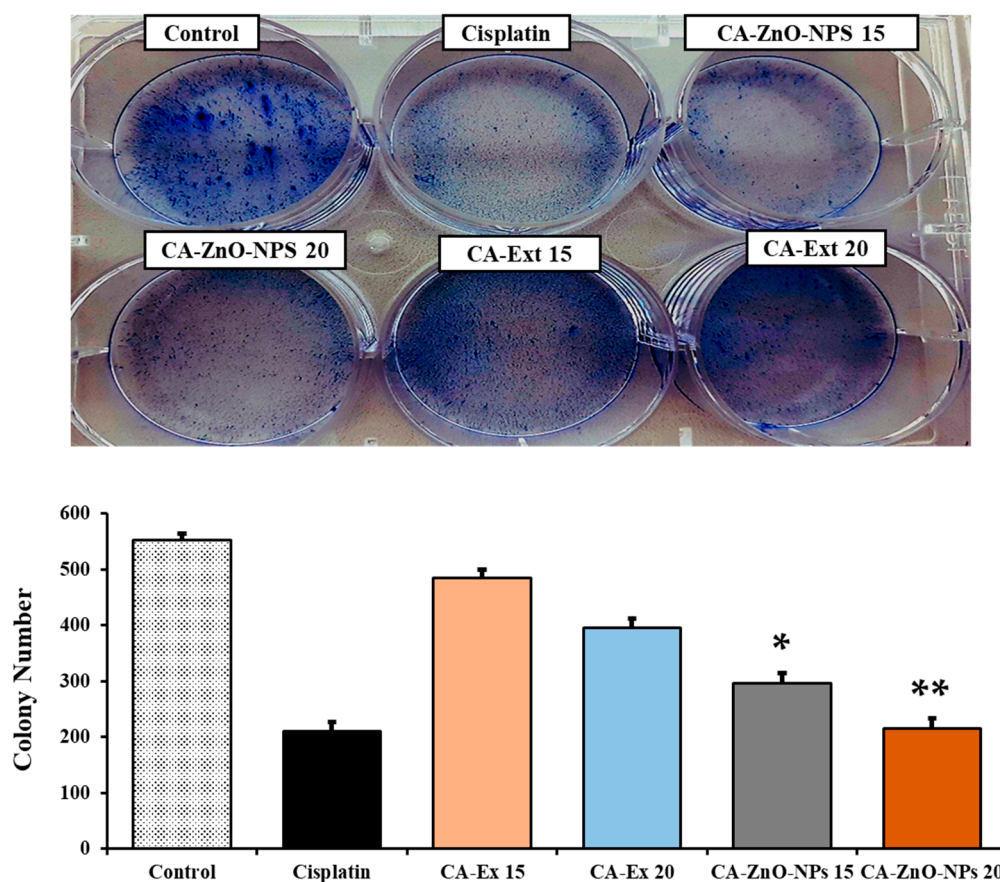


**Figure 9.** Colony formation assay in A549 lung cancer cells at 15 and 20  $\mu\text{g}/\text{mL}$  concentrations of cisplatin, CA extract, and CA-ZnO NPs. Corresponding bar graph of colony formation assay showing the number of colonies/dish when A549 cells were treated with cisplatin (20  $\mu\text{M}$ ), CA extract, and CA-ZnO NPs. \*  $p < 0.05$ ; \*\*  $p < 0.001$  indicates significant differences from control groups.

### 3.10. CA-ZnO NPs Inhibit Migration of Cancer Cells

The majority of cancers are genetically predisposed; mutations can cause normal cells to acquire malignant characteristics, turning them into cancerous cells. Genome instability and mutations, one of which is the ability of tumor cells to penetrate and spread, dictate the characteristics of cancer [47]. The primary factor in cancer-related death is metastasis. Tumor cells travel throughout the body during the metastasis process, creating secondary sites and severely impairing organ function [48]. A major goal of cancer treatment is to avoid the spread of cancer because it causes 90% of all cancer-related deaths [49]. The in vitro wound-healing scratch test assay is the most popular for evaluating the percentage of cell migration for cancer cell types. The A549 lung cancer cells were treated with cisplatin (20  $\mu\text{M}$ ), CA-Ex (15, 20  $\mu\text{g}/\text{mL}$ ), and CA-ZnO NPs (15, 20  $\mu\text{g}/\text{mL}$ ) in this assay to assess cell movement (%) before and after the treatment (Figure 10A,B). When compared to the positive control and untreated groups, cells treated with CA-ZnO NPs exhibited reduced migration after 1 day at a dosage of 20  $\mu\text{g}/\text{mL}$ . Following 24 h, the control group had almost all of the gaps between layers filled in by migratory cells. Additionally, cancer cells treated with CA-Ex were less able to prevent migration compared to those treated with nanoparticles and the control group. The findings of these studies suggest that CA-ZnO NPs showed the ability to inhibit migration and overall help to stop the metastasis of cancer cells.

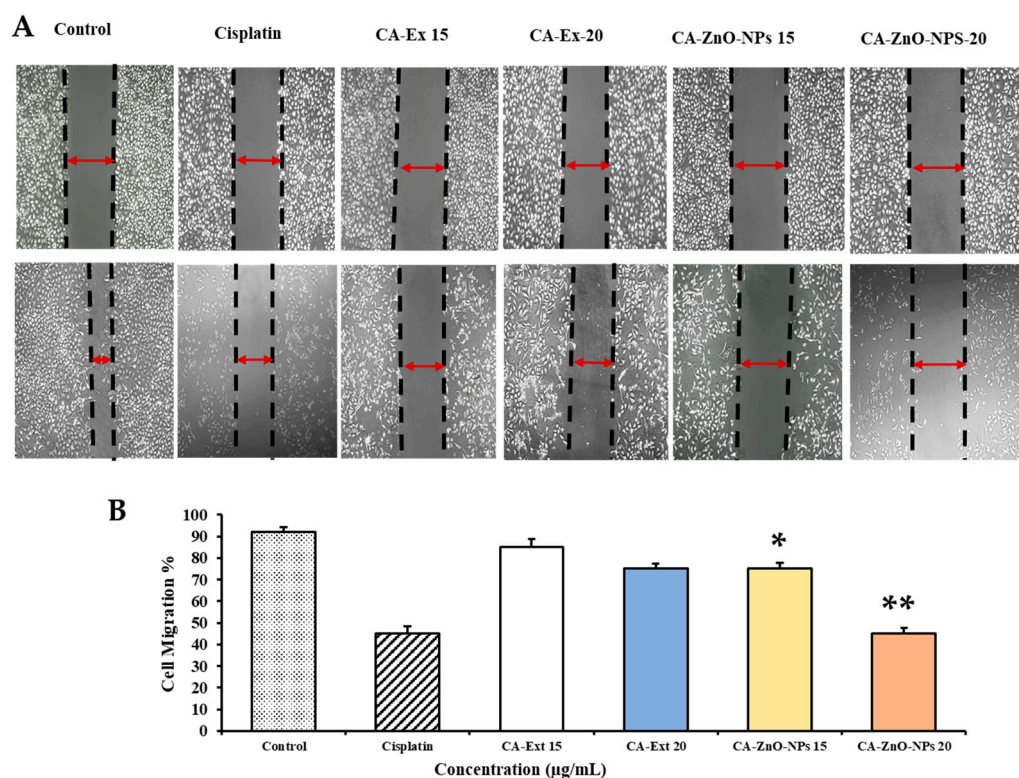


**Figure 10.** (A) Image J software was used to calculate the cell-free area of the scratched region. (B) The fraction of scratch cell migration seen 24 h after treatment compared to control values indicates the quantity of cell migration. Untreated cells are shown as controls. The values are presented as mean and standard deviation, with statistical significance denoted as \*  $p < 0.05$  and \*\*  $p < 0.01$ . The scale bar indicates 10× magnification.

### 3.11. Investigation of CA-ZnO-NP-Induced Apoptosis by Hoechst-33342/PI Dye Staining

Biosynthesized metal oxide nanoparticles (MONPs) are reported to induce apoptosis in anticancer activity [50]. The production of ROS by MONPs is the primary cause of the triggering of apoptosis. ROS production causes oxidative stress. The cell proteins are denatured and lipids are oxidized in response to this oxidative stress. Afterward, DNA is damaged, necrosis occurs, and cells die through apoptosis [51]. The morphological changes that follow from apoptosis in cells may be used to determine thoroughly whether apoptosis has occurred. Among the specific changes are shrinkage of the cell, chromatin condensation, and fragmentation of the cytoplasm or nucleus. A Hoechst dye (HO) and propidium iodide (PI) dual-staining investigation was carried out to validate the induction of apoptosis in A549 cells with cisplatin, CA-Ex, and CA-ZnO NPs after the treatment time of 24 h. While HO staining can show healthy cells (light blue) or early apoptotic cells (dark blue) with fragmented DNA, PI staining can show dead cells (dark red). The number of cells began to decline when 15 µg/mL of CA-ZnO NPs was added to the cells (Figure 11A,D) in comparison with the control and cisplatin. After PI staining, a significant proportion of dead cells was visible for 20 µg/mL of CA-ZnO NPs (Figure 11B,E). In the cells treated with CA-ZnO NPs at 20 µg/mL, the number of necrotic cells increased, as determined at higher magnification, and nuclei and cell shape were changed, as shown in merged images (Figure 11C,F). These results highlighted that after CA-ZnO NP treatment in different concentrations, the cell membrane shattered, allowing the dye to penetrate the injured cell and stain the nucleus, demonstrating that apoptosis was the cause of cell death.

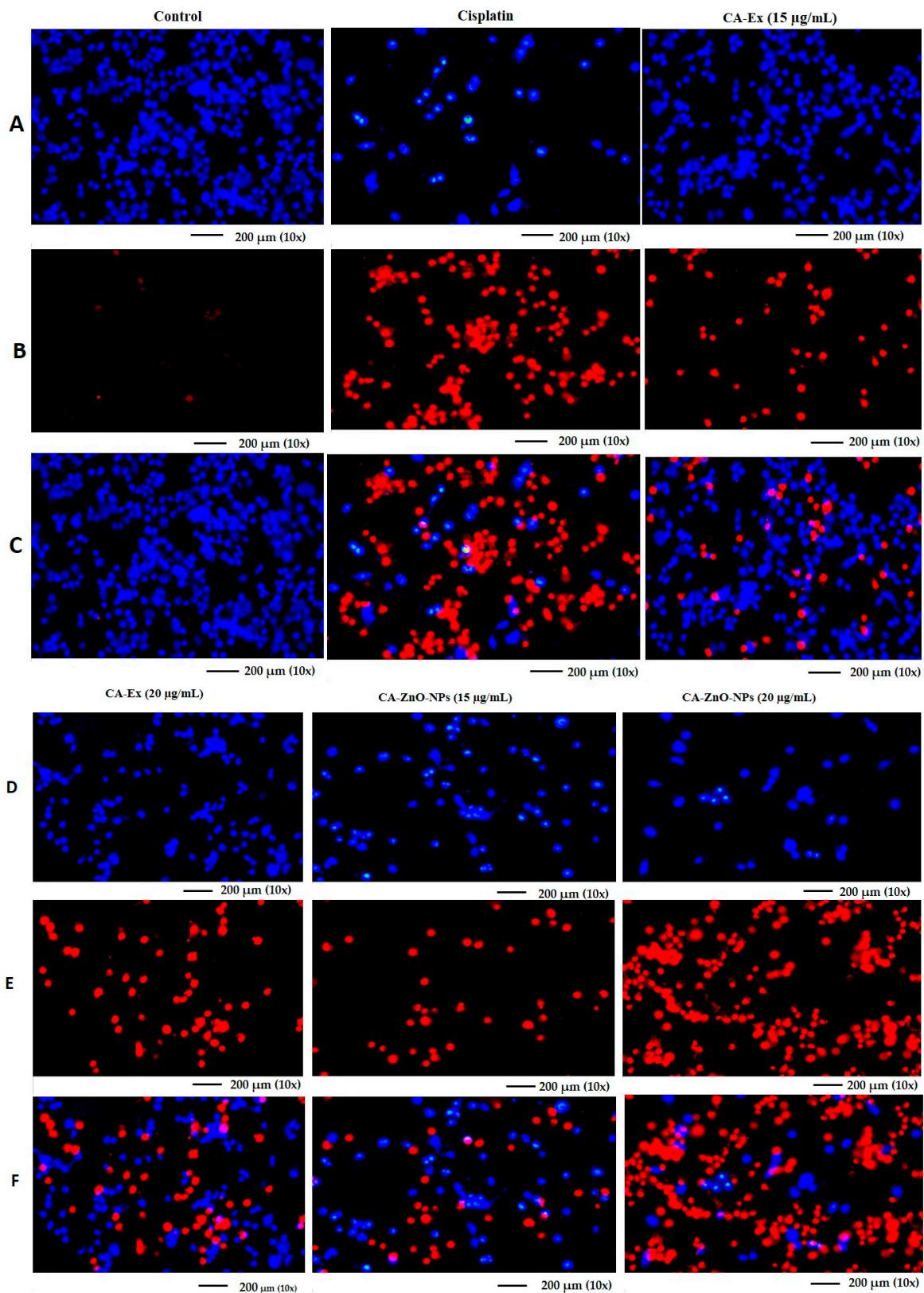


**Figure 11.** Samples were stained with Hoechst and PI, and cellular apoptosis was detected by observing cell disruption and cell wall breakdown. (A,D) Hoechst staining (light-blue live cells and dark-blue apoptotic cells), (B,E) PI staining (dark-red dead cells), and (C,F) merged images. The scale bar is 200 µm (original magnification 10 ×).

### 3.12. By Controlling Apoptotic Gene Expression, CA-ZnO NPs Induced Apoptosis

An essential part of a body's metabolic process is apoptosis, which is a general mechanism for cell death. The growth of a tumor cell is unrestrained, and it resists apoptosis as it develops [52]. In order to destroy tumor cells, anticancer mediators are important for stimulating apoptosis. An effective antitumor agent destroys or blocks cancer cell replication by activating apoptosis [53]. Phytochemicals activate a variety of intracellular stimuli when they stimulate apoptosis via the intrinsic apoptotic pathways. ROS generated by mitochondria are crucial for redox signaling, while p53 suppresses cancer through its redox-active nature. Due to the activation of p53 by ROS, cancer cells undergo apoptosis [54]. Bax and bcl2 are two pro- and anti-apoptotic genes whose expression is regulated by p53 [55]. Bax can cause apoptosis when its expression is elevated, but Bcl-2 can prevent apoptosis when its expression is decreased [56]. A variation in the range of those proteins damages the mitochondrial membrane, which triggers the release of cytochrome c and regulates the activation of caspase-9 [57]. One of the most significant classes of proteases, caspases, plays a key role in cell death. Bax protein, a crucial component of the mitochondrial membrane, aids in the movement of cytochrome c between the membranes, resulting in the development of apoptotic remnants, and it activates caspase-9 and caspase-3, which in turn cause apoptosis [58]. Furthermore, qRT-PCR (Figure 12A–F) demonstrated a dose-dependent elevation of p53 (1.61-fold) and bax (1.72-fold), caspase 3 (1.82-fold), caspase 9 (1.99-fold), and Cyto C (0.162-fold) and downregulation of bcl2 (0.53-fold) gene expression caused by CA-ZnO NPs at 20  $\mu\text{g}/\text{mL}$  in comparison to the commercial medication cisplatin. As a result, our study demonstrated that CA-ZnO NPs can prevent lung cancer cells from expressing an apoptosis gene. To completely comprehend the biological pathways, further study of molecular mechanisms and Western blot analysis are needed.

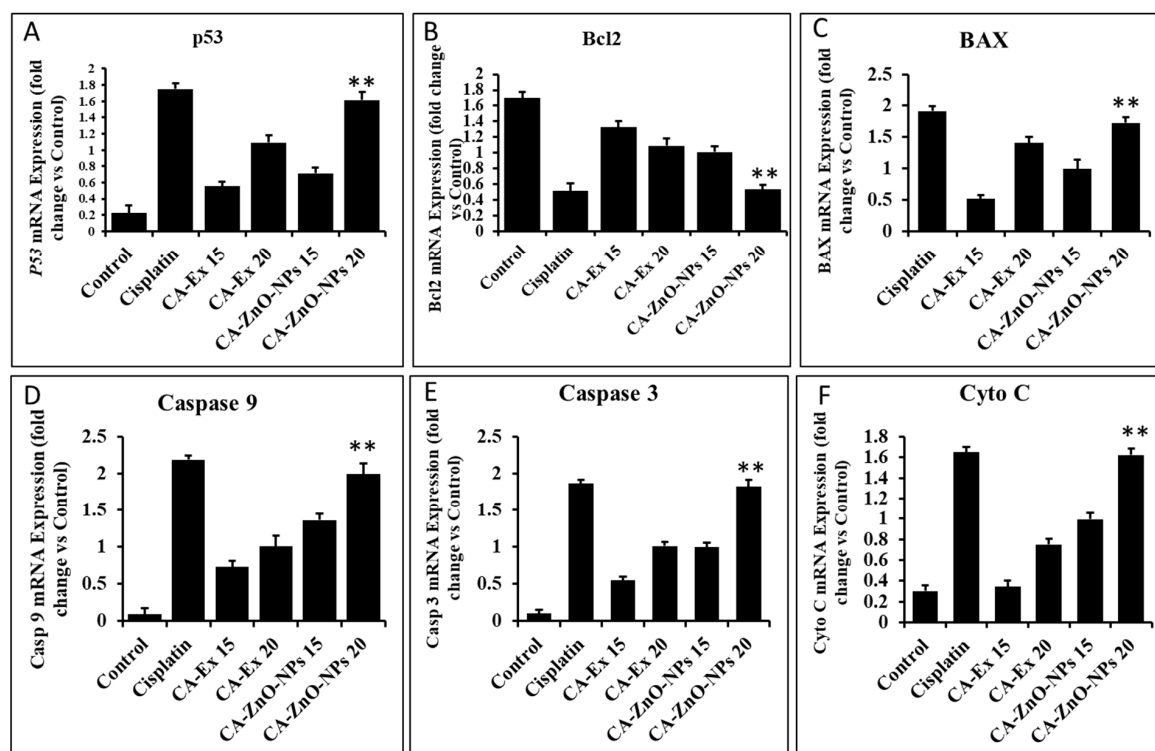


**Figure 12.** Effects of cisplatin, CA extract, and CA-ZnO NPs on the levels of mRNA expression of apoptosis-related genes in A549 cells. Cisplatin (20  $\mu\text{M}$ ), CA extract, and CA-ZnO NPs were applied to A549 cells at concentrations of 15 and 20  $\mu\text{g}/\text{mL}$  for 24 h. (A) p53, (B) BAX, (C) Bcl-2, (D) caspase 9, (E) caspase 3, and (F) Cyto C. Each bar displays the mean  $\pm$  SE of duplicate samples from 3 independent experiments (\*\*  $p < 0.01$  using Student's *t*-test compared to the non-treated control).

### 3.13. CA-ZnO NPs Increased NO Production while Inhibiting ROS Generation Caused by LPS

Nanoparticles have undergone substantial research as a possible anti-inflammatory drug in recent years. Nanoparticles have greater surface-reactive qualities as a result of their high surface-area-to-volume ratio, which leads to more contact with the cell membrane and simpler transport within the membrane [59]. Because of their nanoscale size, ZnO NPs can easily pass through biological membranes. Zinc oxide nanoparticles have been shown in prior research to have strong anti-inflammatory properties [60]. The nitric oxide synthase (NOS) enzyme also uses l-arginine and oxygen as substrates, whereas NADPH and Ca<sup>2+</sup> are employed as co-factors to produce nitric oxide (NO). NO is a free radical that signals cells and is crucial in the pathophysiology of many inflammatory diseases. Previous research has shown that NO regulates several inflammatory processes, including leukocyte rolling and transmigration, the transcription of pro-inflammatory genes, and the modulation of vascular responses [61]. Lipopolysaccharide (LPS) is a powerful suppressor of NOS expression and, as a result, a key regulator of NO generation. Nitric oxide (NO) generation that is excessively high is a typical feature of inflammatory disorders [62]. Accordingly, we examined how zinc salt (10 µg/mL), CA-Ex, and CA-ZnO NPs (0–30 µg/mL) affected the ability of murine macrophages to produce NO. At 20 µg/mL concentration, CA-ZnO NPs showed significantly stronger inhibition of LPS-induced NO production (approximately 54.57%) in comparison to CA-Ex (30.46%) (Figure 13A). L-NMMA was utilized as a positive control in this investigation to inhibit NO production. In contrast, oxidative metabolism is essential for cellular viability. The body’s immune system will overproduce reactive oxygen species (ROS) during inflammation and cause an imbalance in the antioxidant state, which can damage DNA, proteins, lipids, and other biomolecules. This process generates free radicals and ROS, which may have some unwanted effects [63]. RAW 264.7 cells were treated with zinc salt (10 µg/mL), CA-Ex, and CA-ZnO NPs in the presence of LPS to assess the inhibitory effects of samples on LPS-induced ROS generation. The amount of ROS produced increased in the LPS-treated group compared to the control group; therefore, CA-ZnO NPs suppress ROS production in a dose-dependent manner (Figure 13B).

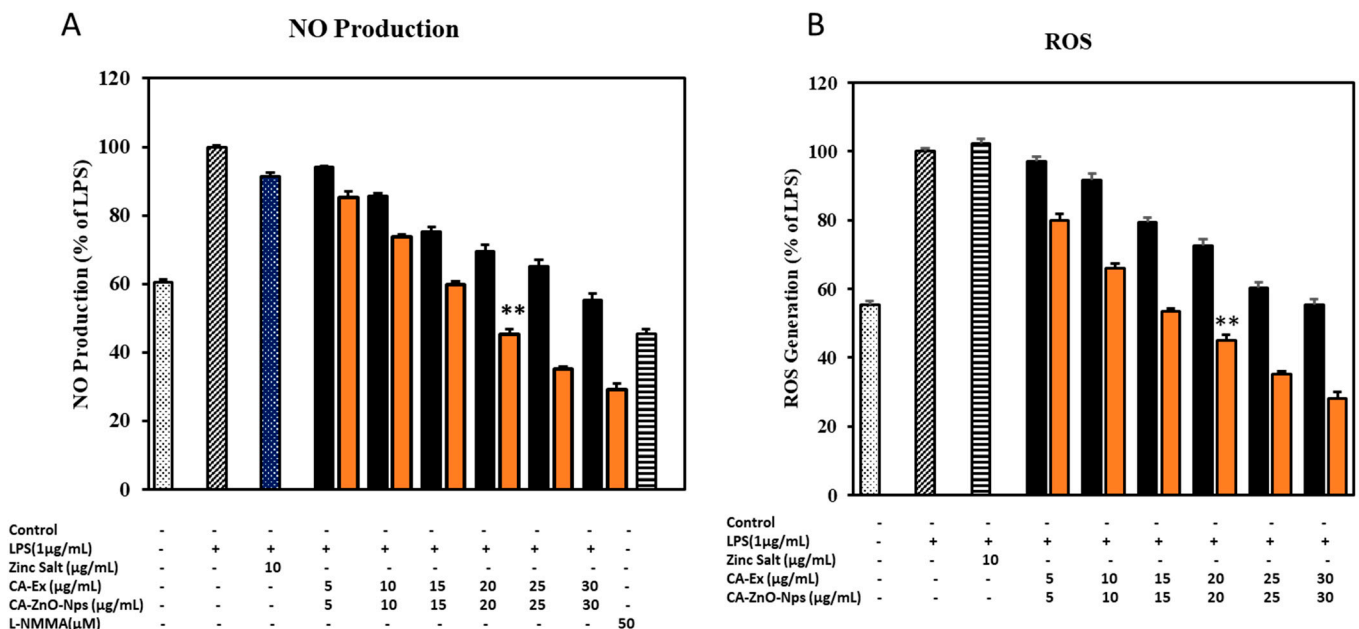


**Figure 13.** The effects of zinc salt, CA extract, and CA-ZnO NPs on (A) NO generation, as measured in RAW 264.7 cells stimulated with 1 µg/mL LPS, and (B) the generation of intercellular ROS, as compared to a control. Data presented as ±SEM, \*\* *p* < 0.01 vs. control cells. All treatments were performed three times.

### 3.14. The Effect of CA-ZnO NPs on Inflammatory Cytokines

Inflammation, which can be either acute or chronic, is a crucial component of the innate immune system [64]. Pro-inflammatory mediators have a significant role in the development of inflammatory disorders [65]. An excessive inflammatory response can also induce inflammation that is persistent and damages healthy tissue. The crucial mediators of skin inflammatory responses include IL-6, IL-8, TNF- $\alpha$ , and COX-2 [66]. Macrophages that have differentiated from monocytes employ the nuclear factor-B (NF- $\kappa$ B) and mitogen-activated protein kinase (MAPK) signaling pathways to activate genes implicated in inflammation. Tumor necrosis factor-alpha (TNF- $\alpha$ ), interleukin-1beta (IL-1  $\beta$ ), cyclooxygenase-2 (COX-2), and IL-6 are among the target genes that the activated NF- $\kappa$ B binds to in the nucleus [67]. We investigated whether CA-Ex and CA-ZnO NPs can suppress the production of pro-inflammatory cytokines as well as the expression levels of these genes using qRT-PCR. Accordingly, after treatment with LPS, the mRNA expression levels of COX-2, TNF- $\alpha$ , iNOS, IL-6, and IL-8 were subsequently increased. In contrast, at 20  $\mu$ g/mL, CA-ZnO nanoparticles significantly suppressed the mRNA level of COX-2 (0.90-fold), TNF- $\alpha$  (0.60-fold), iNOS (0.82-fold), IL-6 (0.62-fold), and IL-8 (0.92-fold) when compared to the same concentration of the CA extract (Figure 14). Therefore, the quantity analysis showed that CA-ZnO NPs have a greater ability to suppress inflammation in LPS-treated macrophage cells.

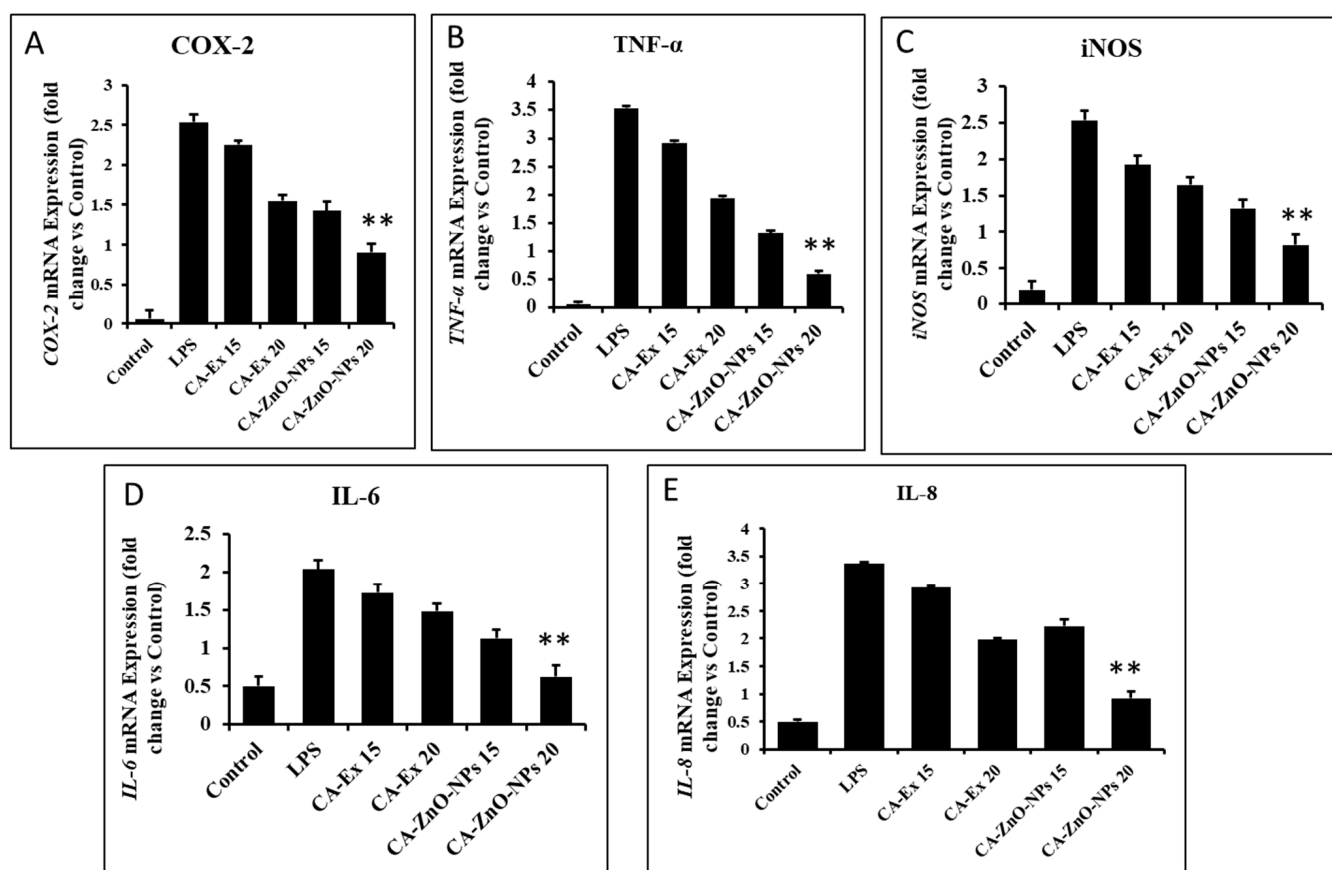


**Figure 14.** Effects of CA extract and CA-ZnO NPs on pro-inflammatory mediators (A) COX-2, (B) TNF- $\alpha$ , (C) iNOS, (D) IL-6, and (E) IL-8 in LPS-induced RAW 264.7 cells. qPCR analysis was used to evaluate mRNA expression. Data presented as  $\pm$ SEM, \*\*  $p < 0.01$  vs. normal. All treatments were performed three times.

#### 4. Conclusions

Plant-synthesized ZnO NPs are outstanding and are being used more frequently in the treatment of cancer and inflammation. With their ability to target cancer cells specifically and their usefulness as carrier agents, ZnO nanoparticles can be an effective alternative to current cancer treatments. According to this study, the formation of intracellular ROS greatly increased the cytotoxicity of CA-ZnO NPs on human lung cells, which may influence the mechanical mechanism of cell survival. Hoechst and PI staining findings demonstrated that NPs caused cancer cells to undergo apoptosis. In addition, qRT-PCR was used to establish that cancer cells undergo cellular death via the intrinsic mitochondrial route at the gene expression level. Additionally, CA-ZnO NPs boosted p53, Bax, Casp 3, and Casp 9 expression while suppressing Bcl-2 gene expression. As a result, the in vitro study also revealed that CA-ZnO NPs are less hazardous to RAW cells when compared to the commercial drug cisplatin, decreasing the production of pro-inflammatory mediators such as COX-2, TNF- $\alpha$ , iNOS, IL-6, and IL-8 while also inhibiting NO synthesis and intercellular ROS formation. These findings collectively suggest that CA-ZnO NPs have the potential to be extremely effective anti-lung-cancer and anti-inflammatory medicines.

**Author Contributions:** Conceptualization, D.-C.Y., D.-U.Y., D.-H.J. and S.-K.J.; methodology, J.N., E.J.R., M.A., M.M., M.A.-A. and J.-K.P.; software, J.N., E.J.R., M.M., M.A. and L.L.; validation, E.J.R., D.-C.Y. and D.-U.Y.; formal analysis, J.N., M.A.-A., E.J.R., M.A. and J.-K.P.; resources, D.-U.Y., I.M.K., and S.-J.L.; data curation, E.J.R., J.N., M.A. and L.L.; writing—original draft preparation, J.N., E.J.R. and M.A.; writing—review and editing, J.N., E.J.R. and D.-U.Y.; supervision, D.-C.Y., D.-U.Y., D.-H.J. and S.-K.J.; project administration, D.-C.Y., D.-U.Y., D.-H.J. and S.-K.J. All authors have read and agreed to the published version of the manuscript.

**Funding:** This research did not receive any external funding.

**Institutional Review Board Statement:** Not applicable.

**Informed Consent Statement:** Not applicable.

**Data Availability Statement:** The data will be provided only by Dr. Esrat Jahan Rupa.

**Conflicts of Interest:** Author Seung-Jin Lee was employed by the company Nature Bio Pharma Co., Ltd. And Authors Deok-Chun Yang and Dong-Uk Yang were employed by the company Hanbangbio Inc. The remaining authors declare that the research was conducted in the absence of any commercial or financial relationships that could be construed as a potential conflict of interest.

#### References

1. Medzhitov, R. Inflammation 2010: New adventures of an old flame. *Cell* **2010**, *140*, 771–776. [[CrossRef](#)] [[PubMed](#)]
2. Nathan, C.; Ding, A. Nonresolving Inflammation. *Cell* **2010**, *140*, 871–882. [[CrossRef](#)] [[PubMed](#)]
3. Takeuchi, O.; Akira, S. Pattern recognition receptors and inflammation. *Cell* **2010**, *140*, 805–820. [[CrossRef](#)]
4. Kumar, D.; Bhat, Z.A.; Singh, P.; Bhujbal, S.S.; Mudgade, S.C.; Deoda, R.S. Antiallergic and anti-inflammatory properties of methanolic extract of stem bark of *Ailanthus excelsa* Roxb. *Lat. Am. J. Pharm.* **2010**, *29*, 1289–1295.
5. Kumar, V.; Bhat, Z.A.; Kumar, D.; Khan, N.; Chashoo, I. Evaluation of anti-inflammatory potential of leaf extracts of *Skimmia anquetilia*. *Asian Pac. J. Trop. Biomed.* **2012**, *2*, 627–630. [[CrossRef](#)] [[PubMed](#)]
6. Lavanya, R.; Maheshwari, S.U.; Harish, G.; Raj, J.B.; Kamali, S.; Hemamalani, D.; Varma, J.B.; Reddy, C.U. Investigation of in-vitro anti-inflammatory, anti-platelet and anti-arthritic activities in the leaves of *Anisomeles malabarica* Linn. *Biol. Chem. Sci.* **2010**, *1*, 745–752.
7. Ginwala, R.; Bhavsar, R.; Chigbu, D.G.I.; Jain, P.; Khan, Z.K. Potential role of flavonoids in treating chronic inflammatory diseases with a special focus on the anti-inflammatory activity of apigenin. *Antioxidants* **2019**, *8*, 35. [[CrossRef](#)]
8. Siegel, R.L.; Miller, K.D.; Jemal, A. Cancer statistics, 2018. *CA Cancer J. Clin.* **2018**, *68*, 7–30. [[CrossRef](#)]
9. Bray, F.; Ferlay, J.; Soerjomataram, I. GLOBOCAN estimates of incidence and mortality worldwide for 36 cancers in 185 countries. *CA A Cancer J. Clin.* **2018**, *68*, 394–424. [[CrossRef](#)]
10. US Preventive Services Task Force. Screening for lung cancer: US Preventive Services Task Force recommendation statement. *JAMA* **2021**, *325*, 962–970. [[CrossRef](#)]
11. Lee, S.-B.; Lee, J.-S.; Moon, S.-O.; Lee, H.-D.; Yoon, Y.-S.; Son, C.-G. A standardized herbal combination of *Astragalus membranaceus* and *Paeonia japonica*, protects against muscle atrophy in a C26 colon cancer cachexia mouse model. *J. Ethnopharmacol.* **2021**, *267*, 113470. [[CrossRef](#)] [[PubMed](#)]

12. Alsharairi, N.A. The effects of dietary supplements on asthma and lung cancer risk in smokers and non-smokers: A review of the literature. *Nutrients* **2019**, *11*, 725. [[CrossRef](#)]
13. Jamkhande, P.G.; Ghule, N.W.; Bamer, A.H.; Kalaskar, M.G. Metal nanoparticles synthesis: An overview on methods of preparation, advantages and disadvantages, and applications. *J. Drug Deliv. Sci. Technol.* **2019**, *53*, 101174. [[CrossRef](#)]
14. Zhang, D.; Ma, X.-L.; Gu, Y.; Huang, H.; Zhang, G.-W. Green synthesis of metallic nanoparticles and their potential applications to treat cancer. *Front. Chem.* **2020**, *8*, 799. [[CrossRef](#)] [[PubMed](#)]
15. Xie, B.; Yang, J.; Yang, Q.; Yuan, W. Enantioselective reduction of fluorenones in surfactant-aqueous solution by fruits and vegetables. *J. Mol. Catal. B Enzym.* **2009**, *61*, 284–288. [[CrossRef](#)]
16. Hameed, S.; Iqbal, J.; Ali, M.; Khalil, A.T.; Abbasi, B.A.; Numan, M.; Shinwari, Z.K. Green synthesis of zinc nanoparticles through plant extracts: Establishing a novel era in cancer theranostics. *Mater. Res. Express* **2019**, *6*, 102005. [[CrossRef](#)]
17. Chandrasekaran, S.; Anusuya, S.; Anbazhagan, V. Anticancer, anti-diabetic, antimicrobial activity of zinc oxide nanoparticles: A comparative analysis. *J. Mol. Struct.* **2022**, *1263*, 133139. [[CrossRef](#)]
18. Velsankar, K.; Venkatesan, A.; Muthumari, P.; Suganya, S.; Mohandoss, S.; Sudhahar, S. Green inspired synthesis of ZnO nanoparticles and its characterizations with biofilm, antioxidant, anti-inflammatory, and anti-diabetic activities. *J. Mol. Struct.* **2022**, *1255*, 132420. [[CrossRef](#)]
19. Prashanth, G.; Prashanth, P.; Nagabhushana, B.; Ananda, S.; Krishnaiah, G.; Nagendra, H.; Sathyananda, H.; Rajendra Singh, C.; Yogisha, S.; Anand, S.; et al. Comparison of anticancer activity of biocompatible ZnO nanoparticles prepared by solution combustion synthesis using aqueous leaf extracts of *Abutilon indicum*, *Melia azedarach* and *Indigofera tinctoria* as biofuels. *Artif. Cells Nanomed. Biotechnol.* **2018**, *46*, 968–979. [[CrossRef](#)]
20. Gurib-Fakim, A. Medicinal plants: Traditions of yesterday and drugs of tomorrow. *Mol. Asp. Med.* **2006**, *27*, 1–93. [[CrossRef](#)]
21. Balandrin, M.F.; Kinghorn, A.D.; Farnsworth, N.R. Plant-derived natural products in drug discovery and development: An overview. *ACS Symp. Ser.* **1993**, *534*, 2–12.
22. Yang, D.-C.; Kang, S.C.; Jung, D.-H.; Nahar, J.; Mathiyalagan, R.; Rupa, E.J.; Ramadhania, Z.M.; Han, Y. A Focused Review on Molecular Signalling Mechanisms of Ginsenosides Anti-Lung Cancer and Anti-inflammatory Activities. *Anti-Cancer Agents Med. Chem.* **2022**, *23*, 3–14. [[CrossRef](#)]
23. Liu, X.-Q.; Ickert-Bond, S.M.; Chen, L.-Q.; Wen, J. Molecular phylogeny of *Cissus* L. of Vitaceae (the grape family) and evolution of its pantropical intercontinental disjunctions. *Mol. Phylogenetics Evol.* **2013**, *66*, 43–53. [[CrossRef](#)]
24. Gerrath, J.M.; Posluszny, U. Morphological and anatomical development in the Vitaceae. VI. *Cissus antarctica*. *Can. J. Bot.* **1994**, *72*, 635–643. [[CrossRef](#)]
25. Balasubramanian, P.; Rajasekaran, A.; Prasad, S.N. Folk medicine of the irulas of *Coimbatore forests*. *Anc. Sci. Life* **1997**, *16*, 222–226. [[PubMed](#)]
26. Manokari, M.; Shekhawat, M.S. An updated review on *Cissus vitiginea* L.(Family: Vitaceae)-An important medicinal climber. *World News Nat. Sci.* **2019**, *22*, 75–83.
27. Payani, S.; Bhaskar, M.; Kumar, G.S.; Pradeepkiran, J.A. A study on antimicrobial and anticancer properties of *Cissus quadrangularis* using lung cancer cell line. *Cancer Treat. Res. Commun.* **2023**, *36*, 100732. [[CrossRef](#)]
28. Chauhan, A.; Kumar, A. In-silico Molecular Interaction Studies of Biologically Active Secondary Metabolites of *Cissus quadrangularis* L. as a Potential Anti-cancer Drug. *Int. J. Plant Environ.* **2023**, *9*, 168–171. [[CrossRef](#)]
29. Méndez López, L.F. Metabolomic Profile and Bioassay-Guided Phytochemical Analysis of the Stems from *Cissus trifoliata*, Evaluation of Their Antibacterial and Cytotoxic Activity, and Determination of the Mechanism of Action of One Active Compound. Doctoral Dissertation, Universidad Autónoma de Nuevo León, San Nicolás de los Garza, Mexico, 2020.
30. Purohit, S.; Pancholi, D.; Kunwar, N.; Choudhary, R.; Jain, R. Characterization of AgNPs biosynthesized from stem and leaf extracts of *Cissus quadrangularis* and *C. rotundifolia*. *AIP Conf. Proc.* **2023**, *2752*, 030003.
31. Gupta, A.; Mehta, S.K.; Qayoom, I.; Gupta, S.; Singh, S.; Kumar, A. Biofunctionalization with *Cissus quadrangularis* Phytobioactives Accentuates Nano-Hydroxyapatite Based Ceramic Nano-Cement for Neo-Bone Formation in Critical Sized Bone Defect. *Int. J. Pharm.* **2023**, *642*, 123110. [[CrossRef](#)]
32. Jin, Y.; Huynh, D.T.N.; Myung, C.-S.; Heo, K.-S. Ginsenoside Rh1 Prevents Migration and Invasion through Mitochondrial ROS-Mediated Inhibition of STAT3/NF- $\kappa$ B Signaling in MDA-MB-231 Cells. *Int. J. Mol. Sci.* **2021**, *22*, 10458. [[CrossRef](#)] [[PubMed](#)]
33. Wang, J.-P.; Hsieh, C.-H.; Liu, C.-Y.; Lin, K.-H.; Wu, P.-T.; Chen, K.-M.; Fang, K. Reactive oxygen species-driven mitochondrial injury induces apoptosis by teroxirone in human non-small cell lung cancer cells. *Oncol. Lett.* **2017**, *14*, 3503–3509. [[CrossRef](#)] [[PubMed](#)]
34. Fowsiya, J.; Madhumitha, G.; Al-Dhabi, N.A.; Arasu, M.V. Photocatalytic degradation of Congo red using *Carissa edulis* extract capped zinc oxide nanoparticles. *J. Photochem. Photobiol. B Biol.* **2016**, *162*, 395–401. [[CrossRef](#)] [[PubMed](#)]
35. Goutam, S.P.; Yadav, A.K.; Das, A.J. Coriander extract mediated green synthesis of zinc oxide nanoparticles and their structural, optical and antibacterial properties. *J. Nanosci. Technol.* **2017**, *3*, 249–252.
36. Rupa, E.J.; Kaliraj, L.; Abid, S.; Yang, D.-C.; Jung, S.-K. Synthesis of a zinc oxide nanoflower photocatalyst from sea buckthorn fruit for degradation of industrial dyes in wastewater treatment. *Nanomaterials* **2019**, *9*, 1692. [[CrossRef](#)]
37. Kim, W.J.; Soshnikova, V.; Markus, J.; Oh, K.H.; Anandapadmanaban, G.; Mathiyalagan, R.; Perez, Z.E.J.; Kim, Y.J.; Yang, D.C. Room temperature synthesis of germanium dioxide nanorods and their in vitro photocatalytic application. *Optik* **2019**, *178*, 664–668. [[CrossRef](#)]

38. Bisht, G.; Rayamajhi, S. ZnO nanoparticles: A promising anticancer agent. *Nanobiomedicine* **2016**, *3*, 9. [[CrossRef](#)]
39. Shen, C.; James, S.A.; de Jonge, M.D.; Turney, T.W.; Wright, P.F.; Feltis, B.N. Relating cytotoxicity, zinc ions, and reactive oxygen in ZnO nanoparticle-exposed human immune cells. *Toxicol. Sci.* **2013**, *136*, 120–130. [[CrossRef](#)]
40. Mishra, P.K.; Mishra, H.; Ekielski, A.; Talegaonkar, S.; Vaidya, B. Zinc oxide nanoparticles: A promising nanomaterial for biomedical applications. *Drug Discov. Today* **2017**, *22*, 1825–1834. [[CrossRef](#)]
41. Truong-Tran, A.Q.; Carter, J.; Ruffin, R.; Zalewski, P.D. New insights into the role of zinc in the respiratory epithelium. *Immunol. Cell Biol.* **2001**, *79*, 170–177. [[CrossRef](#)]
42. Sharma, S.; Pujari, P.; Sudarshan, K.; Dutta, D.; Mahapatra, M.; Godbole, S.; Jayakumar, O.; Tyagi, A. Positron annihilation studies in ZnO nanoparticles. *Solid State Commun.* **2009**, *149*, 550–554. [[CrossRef](#)]
43. Rasmussen, J.W.; Martinez, E.; Louka, P.; Wingett, D.G. Zinc oxide nanoparticles for selective destruction of tumor cells and potential for drug delivery applications. *Expert Opin. Drug Deliv.* **2010**, *7*, 1063–1077. [[CrossRef](#)] [[PubMed](#)]
44. Sarmiento-Salinas, F.L.; Perez-Gonzalez, A.; Acosta-Casique, A.; Ix-Ballote, A.; Diaz, A.; Treviño, S.; Rosas-Murrieta, N.H.; Millán-Perez-Peña, L.; Maycotte, P. Reactive oxygen species: Role in carcinogenesis, cancer cell signaling and tumor progression. *Life Sci.* **2021**, *284*, 119942. [[CrossRef](#)]
45. Dröse, S.; Brandt, U. Molecular mechanisms of superoxide production by the mitochondrial respiratory chain. In *Advances in Experimental Medicine and Biology*; Springer: Berlin/Heidelberg, Germany, 2012; Volume 748, pp. 145–169. [[CrossRef](#)]
46. Franken, N.A.P.; Rodermond, H.M.; Stap, J.; Haveman, J.; Van Bree, C. Clonogenic assay of cells in vitro. *Nat. Protoc.* **2006**, *1*, 2315–2319. [[CrossRef](#)] [[PubMed](#)]
47. Hanahan, D.; Weinberg, R.A. Hallmarks of cancer: The next generation. *Cell* **2011**, *144*, 646–674. [[CrossRef](#)]
48. Lambert, A.W.; Pattabiraman, D.R.; Weinberg, R.A. Emerging biological principles of metastasis. *Cell* **2017**, *168*, 670–691. [[CrossRef](#)] [[PubMed](#)]
49. Sikdar, S.; Lallemand, B.; Dubois, J. Induction of phase II enzymes glutathione-s-transferase and NADPH: Quinone oxydoreductase 1 with novel sulfuraphane derivatives in human keratinocytes: Evaluation of the intracellular GSH level. *Pharmacol. Pharm.* **2014**, *5*, 937–943. [[CrossRef](#)]
50. Rani, N.; Saini, K. Biogenic metal and metal oxides nanoparticles as anticancer agent: A review. *Proc. IOP Conf. Ser. Mater. Sci. Eng.* **2022**, *1225*, 012043. [[CrossRef](#)]
51. Valko, M.; Rhodes, C.J.; Moncol, J.; Izakovic, M.; Mazur, M. Free radicals, metals and antioxidants in oxidative stress-induced cancer. *Chem. Biol. Interact.* **2006**, *160*, 1–40. [[CrossRef](#)]
52. Ismail, N.I.; Othman, I.; Abas, F.; Lajis, N.H.; Naidu, R. Mechanism of apoptosis induced by curcumin in colorectal cancer. *Int. J. Mol. Sci.* **2019**, *20*, 2454. [[CrossRef](#)]
53. George, B.P.; Abrahamse, H. Increased oxidative stress induced by *Rubus* bioactive compounds induce apoptotic cell death in human breast cancer cells. *Oxidative Med. Cell. Longev.* **2019**, *2019*, 6797921. [[CrossRef](#)]
54. Liu, B.; Chen, Y.; St. Clair, D.K. ROS and p53: A versatile partnership. *Free Radic. Biol. Med.* **2008**, *44*, 1529–1535. [[CrossRef](#)]
55. Omoyeni, O.A.; Hussein, A.; Meyer, M.; Green, I.; Iwuoha, E. *Pleiocarpa pycnantha* leaves and its triterpenes induce apoptotic cell death in Caco-2 cells in vitro. *BMC Complement. Altern. Med.* **2015**, *15*, 224. [[CrossRef](#)]
56. Kang, M.H.; Reynolds, C.P. Bcl-2 inhibitors: Targeting mitochondrial apoptotic pathways in cancer therapy. *Clin. Cancer Res.* **2009**, *15*, 1126–1132. [[CrossRef](#)]
57. Zheng, J.H.; Viacava Follis, A.; Kriwacki, R.W.; Moldoveanu, T. Discoveries and controversies in BCL-2 protein-mediated apoptosis. *FEBS J.* **2016**, *283*, 2690–2700. [[CrossRef](#)]
58. Li, Y.; Wang, Y.; Yu, X.; Yu, T.; Zheng, X.; Chu, Q. *Radix tetragium* inhibits the non-small cell lung cancer via Bax/Bcl-2/Caspase-9/Caspase-3 pathway. *Nutr. Cancer* **2022**, *74*, 320–332. [[CrossRef](#)]
59. Agarwal, H.; Shanmugam, V. A review on anti-inflammatory activity of green synthesized zinc oxide nanoparticle: Mechanism-based approach. *Bioorganic Chem.* **2020**, *94*, 103423. [[CrossRef](#)]
60. Rajakumar, G.; Thiruvengadam, M.; Mydhili, G.; Gomathi, T.; Chung, I.-M. Green approach for synthesis of zinc oxide nanoparticles from *Andrographis paniculata* leaf extract and evaluation of their antioxidant, anti-diabetic, and anti-inflammatory activities. *Bioprocess Biosyst. Eng.* **2018**, *41*, 21–30. [[CrossRef](#)]
61. Clancy, R.M.; Amin, A.R.; Abramson, S.B. The role of nitric oxide in inflammation and immunity. *Arthritis Rheum.* **1998**, *41*, 1141–1151. [[CrossRef](#)]
62. Salvemini, D. Regulation of cyclooxygenase enzymes by nitric oxide. *Cell. Mol. Life Sci.* **1997**, *53*, 576–582. [[CrossRef](#)]
63. Wang, Z.; Liu, X.; Bao, Y.; Wang, X.; Zhai, J.; Zhan, X.; Zhang, H. Characterization and anti-inflammation of a polysaccharide produced by *Chaetomium globosum* CGMCC 6882 on LPS-induced RAW 264.7 cells. *Carbohydr. Polym.* **2021**, *251*, 117129. [[CrossRef](#)] [[PubMed](#)]
64. Šoltés, L.; Kogan, G. *Hyaluronan: A Harbinger of the Status and Functionality of the Joint*; Apple Academic Press/Taylor & Francis Group: Burlington, ON, Canada; Palm Bay, FL, USA, 2014; pp. 259–286.
65. Cao, J.; Naeem, M.; Noh, J.-K.; Lee, E.H.; Yoo, J.-W. Dexamethasone phosphate-loaded folate-conjugated polymeric nanoparticles for selective delivery to activated macrophages and suppression of inflammatory responses. *Macromol. Res.* **2015**, *23*, 485–492. [[CrossRef](#)]

66. Yang, M.; Wang, Y.; Patel, G.; Xue, Q.; Njateng, G.S.S.; Cai, S.; Cheng, G.; Kai, G. In vitro and in vivo anti-inflammatory effects of different extracts from *Epigynum auritum* through down-regulation of NF- $\kappa$ B and MAPK signaling pathways. *J. Ethnopharmacol.* **2020**, *261*, 113105. [[CrossRef](#)] [[PubMed](#)]
67. Park, E.; Lee, S.-M.; eun Lee, J.; Kim, J.-H.J. Anti-inflammatory activity of mulberry leaf extract through inhibition of NF- $\kappa$ B. *J. Funct. Foods* **2013**, *5*, 178–186. [[CrossRef](#)]

**Disclaimer/Publisher's Note:** The statements, opinions and data contained in all publications are solely those of the individual author(s) and contributor(s) and not of MDPI and/or the editor(s). MDPI and/or the editor(s) disclaim responsibility for any injury to people or property resulting from any ideas, methods, instructions or products referred to in the content.